International Journal of Biological Macromolecules 382 (2026) 154518

Contents lists available at ScienceDirect

International Journal of Biological Macromolecules

journal homepage: www.elsevier.com/locate/ijbiomac

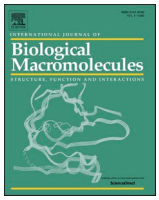

Lightly colored and reactive maleic acid hydrotropic lignin: Characterization and polymeric applications

Xiaoxue Zhang [a,c], Noah Altschuler [b], Linda F. Lorenz [a], Peter Kitin [a], Christopher G. Hunt [a], Hoon Kim [a], Clayton Mickles [a], Jiansong Chen [c], Xuejun Pan [a], J.Y. Zhu [a,c,*]

[a] USDA Forest Products Lab, Madison, WI, 53726, USA
[b] The Potomac School, 1301 Potomac School Road, McLean, VA, 22101, USA
[c] Department of Biological Systems Engineering, University of Wisconsin-Madison, Madison, WI, 53726, USA

ARTICLE INFO

Keywords:
Lignin valorization
Wood adhesive
Sunscreen
Maleic acid hydrotropic fractionation
Solubility
Molecular weight
Chemical structure
Color

ABSTRACT

Acid hydrotropic fractionation using maleic acid, a US FDA approved indirect food additive, can rapidly (20 min) dissolve wood lignin at low temperatures (70–110 °C). This study characterized the physical and chemical properties, i.e., color, molecular weight, solubility, and chemical structure of maleic acid hydrotropic fractionation dissolved wood lignin (MAHL) obtained under various fractionation conditions. The study also demonstrated valorization of MAHL for two polymeric applications through direct mixing with (1) commercial sunscreen for its light color and UV protection capability, and (2) wood adhesives for its good reactivity. Sun protection factor (SPF) values of MAHL-containing sunscreens increased from 14 (control without lignin) upto 205 with just 5 wt% lignin supplementation. MAHL with low carbohydrates and good dispersion in sunscreen produced from moderate fractionation performed best in shielding UV light and yet maintaining light color to meet consumer preference. Lignin phenol formaldehyde (LPF) at 10% MAHL loading can meet the North American standards for interior plywood based on the ASTM D7998 test. MAHL lignin formaldehyde (LF) with phenol formaldehyde (LFPF) at 20% LF substitution resulted in a lignin-based wood adhesive with a wet bonding strength near 6 MPa pressed at 150 °C for 120 s, suitable for interior applications.

1. Introduction

In the context of a circular economy and the global shift toward renewable resources for producing materials and chemicals, lignin in plant biomass has emerged as a promising source of aromatic polymers. As the second most abundant natural polymer after cellulose, its phenolic structure offers great potential for sustainable production of chemicals and advanced polymeric materials. However, lignin valorization remains challenging due to its intrinsic structural complexity and heterogeneity [1]. Its chemical properties not only vary with plant species but also to a greater extent with the extraction methods employed. Whether applying lignin as a polymer or for producing fuels and chemicals through depolymerization, the required lignin properties are great reactivity, light color, and without unpleasant odor. Unfortunately, most lignin extracted from plant biomass, such as commercial technical lignin, deviates significantly from its native structure. The lignin often exhibits highly condensed structures and dark color with odor due to the harsh reaction conditions and chemicals used [1–4]. The condensed lignin structure significantly decreases its chemical reactivity, limiting its potential for producing aromatics through depolymerization [5–8]. This structural rigidity and low reactivity also hamper its utilization as a polymeric material such as a wood adhesive [9] though lignin in nature in its natural state serves as a binder to bond plant cell wall together. Furthermore, the dark color and unpleasant odor of technical lignin restrict its application in personal care products such as sunscreens in which it functions as an anti-UV and antioxidant polymer [10,11]. These examples highlight the challenges in valorizing commercially available lignin, such as industry technical lignin and lignin from various biorefinery fractionation processes.

To mitigate lignin condensation, the strategy of introducing protective chemical groups, particularly through aldehyde-assisted fractionation (AAF) has attracted great interest. This approach stabilizes lignin, preventing undesirable repolymerization and enabling functionalization [5,12]. Remarkably, aldehyde-stabilized lignin has achieved near-theoretical lignin monomer yield upon depolymerization [13]. In addition, the stabilized lignin exhibits a lighter color and demonstrates

* Corresponding author at: USDA Forest Products Lab, Madison, WI, 53726, USA.
E-mail address: junyong.zhu@usda.gov (J.Y. Zhu).

https://doi.org/10.1016/j.ijbiomac.2026.154518
Received 9 February 2026; Received in revised form 9 June 2026; Accepted 13 September 2026
Available online 16 September 2026
0141-8130/Published by Elsevier B.V.

excellent performance in applications such as wood adhesives and surfactants [9,13]. However, implementing AAF typically requires solubilizing lignin in expensive or toxic solvents, such as γ-valerolactone (GVL), dioxane, and tetrahydrofuran (THF), which poses economic and environmental challenges [14,15].

Another promising strategy is reductive catalytic fractionation (RCF), which enables efficient depolymerization of lignin into valuable aromatic monomers [6,16]. Often referred to as a "lignin-first" biorefining approach, RCF prioritizes lignin processing in a single step to achieve high yields of lignin-derived aromatics. However, this method typically requires elevated temperatures and pressures, along with transition metal catalysts, resulting in substantial capital and operating costs [17]. Moreover, the harsh reductive reaction conditions pose challenges for the concurrent valorization of carbohydrate fraction, which is often degraded or neglected during processing. This limitation significantly impacts the overall economics of biorefineries, as carbohydrates constitute approximately two-thirds of lignocellulosic biomass.

Various approaches have been explored to obtain light-color lignin, including UV-irradiation [18], fractionation techniques such as membrane ultrafiltration [19], mechanical grinding [20], and solvent-based fractionation [21,22]. Thermal treatment was also found effective in activating lignin, resulting in light-color and reactive lignin [23,24]. Additionally, chemical treatments, such as sulfonation [25] and demethylation [26] have been employed to reduce lignin color. These physical, thermal, and chemical processes were primarily focused on producing lignin with light color for color sensitive applications such as sunscreens. However, the reactivity of the resultant lignin has not been thoroughly investigated in the context of repolymerization into a final product, such as curing of an adhesive, and depolymerization to produce aromatics. Furthermore, post-fractionation treatments introduce an additional processing step and increase overall cost. In addition, processes such as thermal activation are conducted at elevated temperatures over 250 °C, making them energy-intensive and costly. Similarly, fractionation methods that rely on organic solvent systems often result in low product yield, posing further economic and environmental challenges.

In view of the limitations of existing processes for producing light-color and reactive lignin, producing such lignin directly from plant biomass through novel fractionation processes—without post-fractionation treatment or additional fractionation steps—offers a promising route to reduce production cost. One such approach is the one-pot AAF [17]. Notable success has been achieved using organic solvents such as γ-Valerolactone (GVL). For example, a lignin yield of approximately 40% of theoretical was achieved at 100 °C for 1 h with the resulting poplar wood lignin retaining 33% β–*O*–4 linkages, compared with 69% in native poplar lignin [27]. However, the high cost of GVL remains a major barrier to commercial-scale implementation.

In this context, we introduce maleic acid (MA) hydrotropic lignin (MAHL) as a potentially viable feedstock for high value lignin valorization. The acid hydrotropic fractionation ((M)AHF) process, recently developed by the Zhu's lab at the USDA Forest Products Laboratory [28,29], has attracted great attention [30–32]. Unlike the salt based hydrotropic systems [33,34], which require high temperatures and long reaction times, acid-based AHF can rapidly solubilize lignin within approximately 20 min at relatively low temperatures of 70–110 °C, while simultaneously producing a readily digestible cellulose-rich substrate suitable for enzymatic saccharification at low enzyme dosages [35]. In AHF, lignin is solubilized in water in two steps: hydrolysis of hemicelluloses to break the lignin-carbohydrate complexes (LCCs) and cleavage of lignin ether linkages by the acid hydrotrope, then solubilizing the cleaved lignin in water through hydrophobic aggregation by the hydrotrope at above the minimum hydrotropic concentration [28]. The ether cleavage generates additional phenolic hydroxyl groups, which initiate further reactions such as condensation or crosslinking (e.g., with formaldehyde in adhesive systems and forms formaldehyde bridge linkages) to increase MAHL reactivity. In addition, MAHF decreases molecular weight through depolymerization which improves accessibility of reactive sites by generating more phenols. The use of MA as an hydrotrope—an FDA-approved weak dicarboxylic acid as an indirect food additive under 21CFR175–177—offers substantial environmental advantages over organic solvent-based fractionation processes. Additionally, limited water solubility of MA enables simple and efficient acid recovery via crystallization [35], thereby enhancing both the sustainability and economic feasibility of the process. Our past work on maleic acid hydrotropic fractionation (MAHF) were primarily focused on sugar and cellulose nanomaterials production [29,35,36], along with evaluation the UV-shielding properties the MAHL itself [37]. However, there is no work reported on applications of MAHL for formulating wood adhesives and sunscreens. On this ground, the present study is novel.

The objectives of the present study are twofold: (1) to characterize the physical properties and chemical structures of MAHL to support its effective utilization, and (2) to demonstrate its unique potential in two polymeric applications—sunscreens, leveraging its light color and UV-blocking capability, and wood adhesives, using its high chemical reactivity and natural capability in bonding plant cell walls to offer a sustainable alternative to petroleum derived phenol in wood adhesives [9]. Among various lignin valorization pathways, polymeric applications have been identified as the most economically and technologically promising pathway for lignin valorization [17,38]. Given the robust performance of maleic acid hydrotropic fractionation (MAHF) in terms of process intensity, i.e., rapid fractionation at low temperatures and effective cell wall deconstruction that yields a readily digestible cellulosic substrate, this study on MAHL holds practical significance. It contributes to advancing plant biomass utilization and accelerating the commercialization of biorefinery technologies, thereby supporting the transition from a petroleum-based economy to a bio-based circular economy [39].

2. Experimental

2.1. Materials

Commercial birch wood chips were supplied by a pulp mill in Canada. The chips were first subjected to steam pretreatment at 134 °C (or 30 psi) for 8 min and then directly fed into a pressurized 12-inch disk refiner (Andritz Sprout-Bauer Pressurized Refiner, Andritz Sprout, Muncy, PA) with a disk plat gap of 0.25 mm to produce thermomechanical pulp (TMP) fibers. The resultant TMP was air-dried in ambient conditions for 24 h to reach a solids content of approximately 73 wt%, then stored in a refrigerator until use.

The chemicals used in this study included anhydrous MA, phenol with >99% purity, paraformaldehyde with 95% purity, and sodium hydroxide with purity ≥98%, purchased from Sigma-Aldrich (St. Louis, MO, USA).

3M™ Transpore™ Surgical Tape (1527 Series, Solventum Corporation, USA) was used as a substrate to simulate human skin for sunscreen application testing. A commercial SPF 15 mineral sunscreen (3 oz, Absolutely Natural, USA) was purchased from Amazon. This product is water-resistant with broad-spectrum protection and formulated for use on both body and face.

2.2. MA hydrotropic fractionation

MAHF experiments were carried out using an 800-mL flow-through reactor with 200-mesh steel screens at both the inlet and outlet, as described elsewhere [40] and illustrated in the schematic flow diagram (Fig. 1). 100 g in oven-dry (OD) weight of birch TMP or aspen wood flour were preloaded into the reactor and heated to the target fractionation temperature of 110 °C in a sand bath. Aqueous MA solutions (35 and 50 wt%) were first pumped into the reactor at a high flow rate of 200 mL/min for 4 min using a peristaltic pump (WZ1R057, Masterflex, Vernon, IL), to rapidly flood the biomass to decrease the initial transient time.

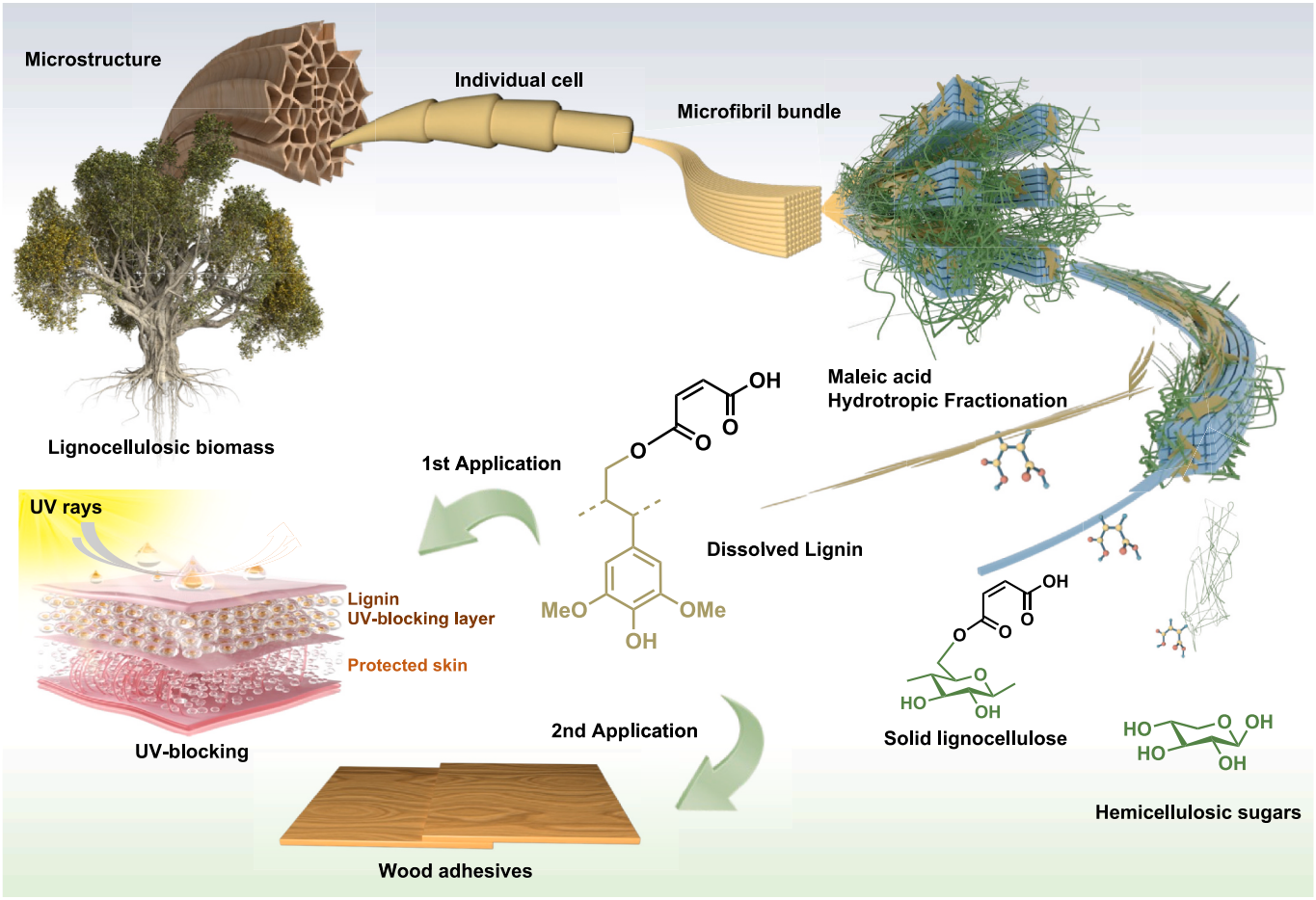

Fig. 1. Schematic diagram of the flow-through maleic acid hydrotropic fractionation (MAHF) process and subsequent analytical characterizations and polymeric applications.

The flow rate was then lowered to 40 mL/min to conduct flow through fractionation for 20 min. As a result, the total MA solution to biomass ratio was kept at 16 for all experiments. The spent MA liquor exiting the reactor was immediately cooled down by flowing into a beak loaded with a known amount of ice to prevent condensation reactions of the dissolved lignin. Aliquots of spent liquor were collected every 3 min to obtain time-dependent lignin samples. The collected liquor was diluted to below the minimal hydrotropic concentration (MHC) of MA to precipitate the dissolved lignin. At the end of the preset reaction time, the DI water was pumped into the reactor at the flow rate of 200 mL/min to flush the remaining spent liquor. The water insoluble solids (WIS) from fractionation were collected and washed to neutral pH by vacuum filtration.

2.3. Chemical composition analysis

The chemical compositions of the birch TMP and the fractionated WIS were analyzed using the standard two-step acid hydrolysis at the Analytical Chemistry and Microscopy Lab of the USDA Forest Products Laboratory following the National Laboratory of the Rockies procedure [41]. Aliquot solid samples were air-dried and ground to 30 mesh using a Wiley mill, then hydrolyzed and analyzed by ion chromatography. A component mass balance analysis was carried out using the chemical compositions and the yields of the birch TMP and the WIS.

2.4. Lignin purification and characterizations

Dissolved lignin samples were collected and purified through dialysis for characterization and applications. Specifically, lignin in the collected spent liquor was precipitated through diluting the spent liquor to below its MHC at approximately 25 wt% [28,29], and then centrifuged at 10,000*g* for 10 min. The lignin was then transferred into a dialysis tube (Spectrum 132572, Thermal Scientific) with a 10,000 MW cutoff and dialyzed for a few days until pH 6 was reached in the dialysis bag. The dialyzed lignin was freeze-dried for 48 h at −48 °C and 40 Torr.

2.5. Lignin color determination

The color of all freeze-dried lignin samples was measured using a hand-held colorimeter (Model: LS173, Shenzhen Linshang Science & Technology Co., China). The lignin samples were first manually ground to a uniform and fine powder in an agate mortar. Each sample was first evenly spread on a glass slide and covered by a coverslip, and then gently compacted prior to measurements to ensure a uniform and sufficiently thick layer on the glass surface to eliminate background interference. Duplicate measurements were conducted at six positions for each sample. The reported values were the averages with standard deviations. CIE (International Commission on Illumination) values L*a*b* were directly obtained from the colorimeter and converted to RGB values. RGB sliders in Microsoft Excel were used to reproduce the color in a color pad for comparison with the corresponding lignin image [8].

2.6. Lignin dissolution efficiency

The ground lignin sample of 3 mg was transferred to a micro

centrifuge tube, and 1 mL of selected solvent was then added into the tube using a pipette. The mixture was then thoroughly agitated using a digital Orbital Shaker (MS 3, IKA Works, Inc., Wilmington, NC) at 1500 rpm for 250 s. After mixing, the visual appearance of the mixture (clarity/turbidity and the presence of undissolved solids) was recorded by taking photographs under consistent lighting conditions. Representative photographs are shown in Fig. 2. The mixture was then centrifuged at 11,000 rpm for 10 min using a microcentrifuge (Eppendorf® Microcentrifuges 5424). The supernatant was discarded, and the remaining solid was collected and dried at 40 °C in an oven for 24 h. The dried lignin sample was weighed to determine dissolution efficiency (DE) as below.

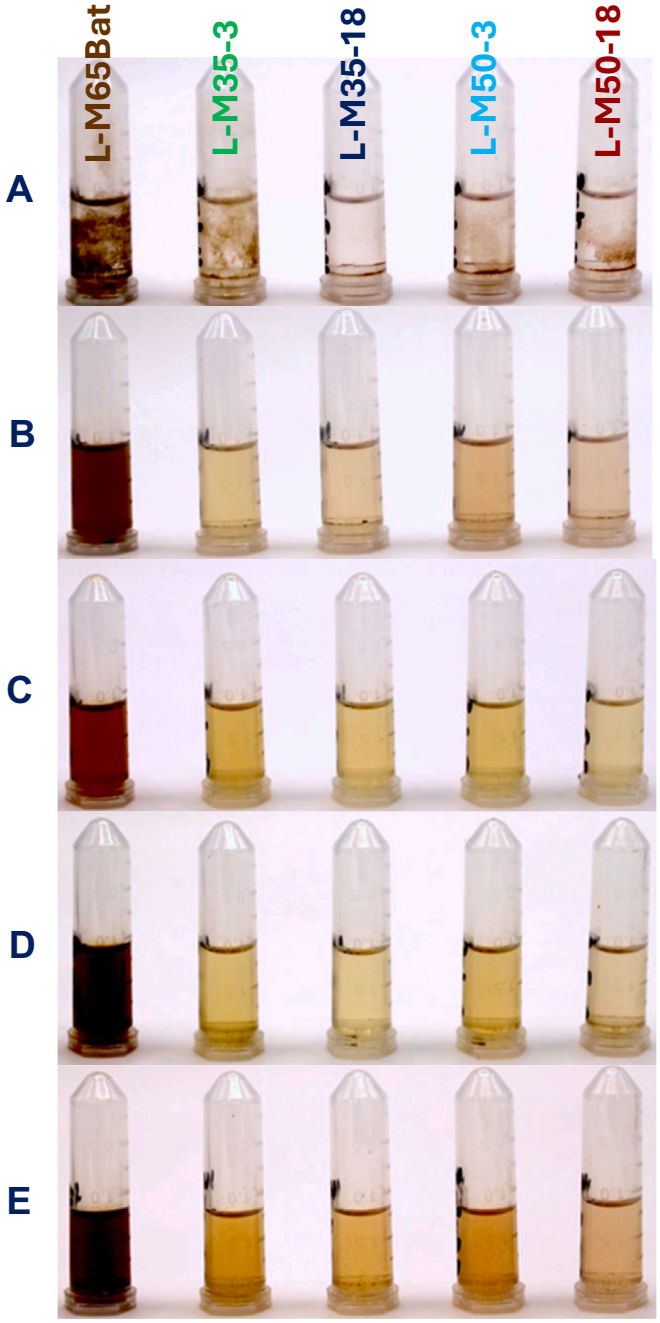

Fig. 2. Photographic comparison of lignin samples dissolved or dispersed in different solvents. A: Hexane; B: Ethanol; C: 1,4-Dioxane; D: Acetone; E: Acetic acid.

$$DE = \frac{M_D}{M_T} \times 100\%$$

where M_D = mass of dissolved lignin (g), M_T = mass of the initial lignin sample. Dissolution experiments were conducted in duplicate, and the reported values are the averages ± standard deviations.

2.7. Lignin molecular weight determination

The number-average (Mn) and weight-average (Mw) molecular weights of lignin samples were determined by gel permeation chromatography (GPC) after acetylation [39]. Lignin samples were acetylated by dissolving 5 mg of each sample in 1 mL mixture of pyridine and acetic anhydride at 1:1 ratio. The mixture was stirred continuously for 12 h in ambient conditions (25 °C). The acetylated lignin was recovered via precipitation in 10 mL of chilled water and subsequent centrifugation. Elution profiles were acquired using a Dionex Ultimate 3000 HPLC system equipped with two Waters Styragel columns (HR 5E and 1) connected in series. A mobile phase of THF was used at a flow rate of 1 mL/min. Acetylated lignin samples were dissolved in THF to a concentration of 0.2 mg/mL and, after filtration through a 0.2 μm membrane, 100 μL was injected into the columns at room temperature. Chromatograms were recorded at 280 nm with a Vanquish Variable Wavelength Detector.

2.8. 2D $^{1}H—^{13}C$ NMR heteronuclear single quantum coherence (HSQC)

The chemical structure of lignin, TMP, and WIS samples were analyzed by 2D $^{1}H—^{13}C$ NMR HSQC method. TMP and WIS samples were first milled using a planetary ball mill (PULVERISETTE 7 premium line, Fritsch, Germany) at 600 rpm with zirconium dioxide (ZrO_2) vessels (20 mL) containing ZrO_2 balls (10 mm diameter ball × 10) and then made to gel-state using a modified DMSO-based protocol [42,43].

Spectra were acquired using a Bruker Avance III HD 500 MHz spectrometer (Bruker Biospin, Billerica, MA), which was equipped with a Prodigy cryo-probe (liquid N2-cooled) featuring a 5 mm gradient TCI probe ($^{1}H/^{13}C/^{15}N$, inverse configuration). Experiments were performed at 298 K. NMR experiments for the whole plant cell wall gel-state samples were performed as previously described [43,44]. About 40 mg of each sample was directly prepared into 5 mm NMR tubes in 0.6 mL of DMSO-d_6:pyridine-d_5 (4:1, v/v). Use of isotopically enriched pyridine-d_5 ("100"; min. 99.94 atom% D) was needed to prevent interference between the residual solvent peaks and aromatic correlations. 2D $^{1}H—^{13}C$ HSQC spectra for TMP and WIS were collected using the Bruker standard pulse sequence 'hsqcetgpsisp2.3.' Data was acquired from 11.0 to −0.5 ppm in F2 (^{1}H) with 1148 data points (acquisition time 100 ms), 215 to −5 ppm in F1 (^{13}C) with 512 increments (F1 acquisition time 9.25 ms) of 111 scans (NS) with a 500 ms interscan delay (D1). The d_{24} delay was set to 0.89 ms (1/8 J, J = 145 Hz). The total acquisition time was approximately 10 h. No shimming process was performed. Lignin samples were acquired with 2298 data points (acquisition time 200 ms), 215 to −5 ppm in F1 (13C) with 512 increments (F1 acquisition time 9.3 ms) of 40 scans with a 1 s relaxation delay (D1). The total acquisition time was approximately 7 h.

Data processing included a matched Gaussian apodization in the direct dimension F2 (LB = −0.1, GB = 0.001) and a squared cosine-bell apodization in the indirect dimension F1 (WDW = QSINE, SSB = 2). Forward linear prediction (one level, 40 coefficients) was applied along F1 to extend the time-domain signal and improve resolution. The central dimethyl sulfoxide-d_6 (DMSO-d_6) solvent peak (δ_C 39.5, δ_H 2.49 ppm) was used as an internal reference.

2.9. Lignin sunscreen preparation and performance evaluation

Lignin samples were first manually ground in an agate mortar.

Lignin-based sunscreens were prepared by dispersing 0.10 g lignin into 1.90 g of the commercial sunscreen using magnetic stirring at 1000 rpm for 24 h at room temperature in the dark, resulting in a lignin loading of 5 wt%. Each lignin-containing sunscreen was applied to a 3M transpore™ tape surface to simulate skin using a 1-mL fine needle syringe for UV transmittance measurements. The sunscreen was then evenly spread across the tape surface at 2 mg/cm^2 loading by gently rubbing with a finger cot. Tape dimensions were 8 mm × 25 mm. Samples were dried in a dark room for 20 min before measurement. The transpore™ tape was affixed on the side of the clean quartz cuvette opposite to the light source. For each sunscreen sample, five non-overlapping spots on the sunscreen applied transpore™ tape were measured with a blank tape as a reference. The reported SPF values are the averages ± standard deviations of five non-overlapping measurements.

The UV transmittances of the lignin-containing sunscreens were measured by a UV–Vis spectrophotometer (UV-3600, Shimadzu, Japan) with an integrating sphere. Five spots were scanned for each sample. In each scan, transmittance (T) per 1 nm was collected in the wavelength range from UVB (290–320 nm) to UVA (320–400 nm). The SPF value was calculated using the following equation:

$$f(x) = \sum_{290}^{400} E_\lambda S_\lambda \Big/ \sum_{290}^{400} E_\lambda S_\lambda T_\lambda$$

where E_λ = CIE erythemal spectral effectiveness, S_λ = solar spectral irradiance, and T_λ = spectral transmittance of the sample [11].

2.10. Light microscopy imaging of sunscreens

A small amount of sunscreen was gently compressed between a microscope glass slide and a cover slip to form a thin layer of evenly spread sunscreen spot. The samples were observed with a light microscope Nikon Eclipse Ci (Nikon Instruments Inc., Tokyo, Japan; Melville, NY) using transmitted (1) bright field, (2) polarized light, or (3) epifluorescence with UV (361–389 nm) excitation and 425 nm long-pass fluorescence emission, and (4) blue (465–495 nm) excitation and 515 long-pass emission. Images were captured with a FLIR Grasshopper 3 (Point Grey) camera in manual mode for comparison of the lignin particles morphology and distribution in different samples. The exposure settings were adjusted to just below saturation.

2.11. Lignin wood adhesive preparation and performance evaluation

Several lignin-based wood adhesives were prepared according to the formulations and conditions listed in Table 1. Due to limited quantities of lignin available, all the lignin samples collected from each fractionation run under M35T110 and M50T110 were combined and used for preparing lignin adhesives for the study. Lignin samples L-MA35 and L-MA50 were separately combined and reacted with formaldehyde at 80 °C for 5 h at a weight-to-weight ratio of 3:1 at pH 2 and then neutralized to pH 7 (Table 1) to produce lignin adhesives (LF).

Table 1
A list of lignin-containing wood adhesive formulations prepared in this study.

Adhesive type	Chemical composition (w/w)	Processing conditions
Lignin and water	75% water +25% lignin	Mixing at room T until well-mixed
Lignin formaldehyde (LF)	25% formaldehyde +75% lignin	Reacting at 80 °C for 5 h. Add more double distilled H_2O when the mixture is running dry
Lignin phenol formaldehyde (LPF)	90% PF + 10% lignin 80% PF + 20% lignin	Mixed and applied to wood
Lignin formaldehyde phenol formaldehyde (LFPF)	90% PF + 10% LF 80% PF + 20% LF	Mixed and applied to wood Mixed and applied to wood

2.12. Differential scanning calorimetry (DSC) testing

The temperature of the cure exotherm and the Delta H of the PF and LPF adhesives were determined by DSC. 10–50 mg of adhesives were added to DSC large volume capsules and sealed (Perkin Elmer DSC 7, Perkin Elmer stainless-steel capsules, Norwalk, CT). Temperature was ramped from 30 °C to 200 °C at 10 degrees/min.

2.13. Automated Bonding Evaluation System (ABES) testing

Bonding was carried out using an Automated Bond Evaluation System (ABES, Adhesive Evaluation Systems, Corvallis, OR, USA) using the methods of ASTM D7998 [45]. Sugar maple (*Acer saccharum*) veneers with a thickness of 0.6 mm were bonded with ~10 mg (100 g/m^2) adhesive applied in a 20 mm by 5 mm overlap area. At least triplicate bonds were formed with 120 s press at each temperature, 150 °C, 160 °C, 180 °C, or 200 °C with a pressure of 1.3 MPa. All samples were stored at 21 °C, 50% RH overnight. Wet samples were then soaked in distilled water for 4 h before testing in shear. Error bars represent standard deviations.

2.14. PF adhesive synthesis

Phenol, formaldehyde, and sodium hydroxide (1:2:0.2 mol ratio) were combined in water at a solids concentration of 50% and reacted at 25 °C for 1 h, then at 85 °C for 45 min plus time to reach a viscosity of 370 to 400 cPs. The mixture cooled quickly to room temperature and stored in a refrigerator.

3. Results and discussion

3.1. Chemical compositions of fractionated wood solids

Lignin samples were produced from birch wood thermo-mechanical pulp (TMP) and aspen wood flour using the MAHF process under different fractionation conditions, labelled as M*xx*T*yyy*t*zz* in Table S1, where *xx*, *yyy*, and *zz* stand for the MA concentration in wt%, fractionation temperature in Celsius, and time in min, respectively. The resulting MAHL was then characterized and evaluated for two polymeric applications as schematically shown in Fig. 1. Yield of MAHL as Klason lignin (KL) increased with increasing MAHF severity in general (Table S1), while solids (fiber) yield decreased. For example, MAHF dissolved approximately 30% of the KL in the least severe flow-through run BM35f (M35T110t18) to approximately 60% of KL in the batch MAHF run AM65b (M65T120t30) using aspen. MAHF also dissolved a significant amount of hemicelluloses (xylan), ranging from about 30% removal in BM35f to approximately 95% in AM65b. In contrast, MAHF preserved most cellulose (glucan), retaining over 80% except in the aspen batch run, indicating minimal cellulose degradation. These results demonstrate that MAHF is highly effective in solubilizing lignin and hemicelluloses while largely preserving cellulose. The run labelled BM50f^ (M50T110t20, Table S1) was a replicate run of BM50f (M50T110t18) with a slightly longer flow-through time of 20 min to demonstrate the repeatability of MAHF. The comparable chemical composition and yield of MA-fractionated WIS from the two runs demonstrate good repeatability of the MAHF process.

3.2. Visual color and appearance of MAHL

The MAHL from each run was precipitated by diluting the spent MA liquor to below the minimal hydrotropic concentration (MHC = 25 wt% [29]). The collected lignin samples are described in Table S2, and their visual color was analyzed. These MAHL samples were labelled as L-M*xx*-*y*, where *xx* and *y* stand for MA concentration in wt% and the liquor

sample collection time in min in the flow-through fractionation, respectively. The MAHL sample with $y = Wa$ represents lignin recovered from the filtrate obtained during the final washing step of the flow-through fractionation. The MAHLs isolated from thermal mechanical pulp (TMP) fibers via MAHF exhibited a broad range of visual appearances, as reflected in their CIE L*ab** color values (Table 2). Overall, their color varied from light beige to deep reddish-brown depending on fractionation severity (Fig. S1). The lightness parameter L* spanned from as high as 87 for sample L-M35-3 to below 56 for L-M50-18 and L-M65Bat, indicating a clear darkening trend with increasing severity of the MAHF conditions. This is due to the increase in the formation of chromophore groups with increasing fractionation severity [8].

MAHL produced from mild to moderate MAHF conditions, e.g., samples L-M35-3 through L-M35-15, retained a light appearance (L* > 70) with L* reaching as high as 87 for L-M35-3. These samples often exhibited pinkish undertones (a* ≈ 6–9, b* ≈ 10–18). Such color characteristics are consistent with the presence of conjugated structures such as Hibbert's ketones and aldehydes (e.g., coniferyl aldehyde), formed through selective β–*O*–4 bond cleavage during acid-catalyzed lignin depolymerization [46,47]. The increase in a* values (redness) together with the decrease in b* values (yellowness) suggest a shift in chromophoric structures from yellow-dominant to more conjugated and reddish species, rather than a simple increase in overall chromophore content, suggesting the presence of chromophores without excessive condensation.

In contrast, MAHLs obtained under more severe fractionation conditions, e.g., L-M50-15 and L-M50-18, exhibited significantly lower L* values (<60) and higher a* values (>11), reflecting darker and more reddish coloration. These trends indicate the onset of lignin condensation reactions at longer fractionation times or higher acid concentrations, which promote the formation of highly conjugated, less soluble lignin structures that absorb more visible light. The color change in MAHLs is associated with the formation of new chromophore structures through condensation, dehydration, and conjugation reactions, as well as from the solubilization of the lignin fragments enriched in these chromophores [48]. Increasing fractionation time and MA produced progressively darker lignin due to the increasing extent of reactions. Consequently, there is a trade-off between MAHL yield and its optical property: i.e., a harsher MAHF condition enhances delignification through great extent of depolymerization to enhance lignin solubilization, and therefore yield, simultaneously promotes structural repolymerization (condensation) due to the reactive linkages made available by depolymerization, along with the formation of chromophore groups which results in color development. Milder MAHF conditions, by contrast, better preserve lignin's light color and reactive structure—desirable for cosmetic applications and for producing high-performance lignin-based materials.

3.3. Solvation of MAHL in organic solvents

The solvation behavior of lignin in different solvents is critical for practical applications and for understanding the structural evolution of lignin during processing. This study focuses on comparative solubility behavior rather than quantitative determination of solubility parameters. Five commonly used organic solvents: hexane, ethanol, 1,4-dioxane, acetone, and acetic acid [49] were selected to evaluate the dissolution behavior of MAHL as shown in Fig. 2. These solvents span a wide range of Hildebrand solubility parameters, polarity, and hydrogen-bonding capabilities, enabling assessment of key physicochemical characteristics of MAHL, including functional group composition, molecular weight, hydrophobicity, and degree of condensation. In general, lignin samples that are lower in molecular weight, less condensed, and enriched in oxygenated functionalities exhibit higher solubility, particularly in solvents of higher polarity and stronger hydrogen bonding capacity. Lignin dissolves most efficiently in solvents with similar Hildebrand solubility parameters to its own.

As summarized in Table 3, acetic acid and 1,4-dioxane showed the highest dissolution efficiency for all MAHL samples, especially for L-M35-18, L-M50-3, and L-M65Bat, with values exceeding 82%. Acetone also demonstrated good solubilizing ability, achieving dissolution efficiency up to 90% for L-M65Bat. These results indicate that MAHL produced under more severe MAHF conditions, such as L-M65Bat, contain highly polar, low-molecular-weight fragments. Polar and highly hydrogen-bonding solvents such as acetic acid, 1,4-dioxane, and acetone can effectively disrupt hydrogen bonding and solubilize lignin fragments enriched with phenolic and other oxygenated functionalities formed during depolymerization and oxidation.

In contrast, hexane, a highly non-polar solvent, dissolved less than 10% of lignin in all cases, reflecting the strongly polar and oxygen-rich nature of MAHL. The extremely poor solubility in hexane also suggests

Table 2
Effect of reaction conditions on the CIE L*a*b* color parameters of the resultant lignin. Color patches were generated based on the measured CIE L*a*b. Values are means ± standard deviations from duplicate measurements at 6 positions for each sample. All lignin samples were dissolved by maleic acid hydrotropic fractionation from birchwood TMP, except L-M65Bat from aspen.

Samples	L*	a*	b*	Color
L-M35-3	87.31 ± 0.36	6.21 ± 0.18	17.66 ± 0.31	
L-M35-6	74.00 ± 0.38	7.68 ± 0.22	11.84 ± 0.27	
L-M35-12	74.15 ± 0.41	8.17 ± 0.20	11.51 ± 0.30	
L-M35-15	76.23 ± 0.36	7.73 ± 0.19	10.74 ± 0.28	
L-M50-3	76.31 ± 0.40	8.79 ± 0.21	10.31 ± 0.25	
L-M50-6	72.26 ± 0.44	10.54 ± 0.26	10.48 ± 0.29	
L-M50-9	67.84 ± 0.39	10.66 ± 0.24	11.11 ± 0.31	
L-M50-12	62.32 ± 0.37	11.64 ± 0.28	10.03 ± 0.27	
L-M50-15	59.34 ± 0.35	12.01 ± 0.30	9.49 ± 0.24	
L-M50-18	59.01 ± 0.33	11.70 ± 0.27	8.55 ± 0.22	
L-M50^-5	69.78 ± 0.41	9.10 ± 0.23	11.69 ± 0.30	
L-M50^-10	62.69 ± 0.38	9.61 ± 0.21	8.58 ± 0.26	
L-M50^-15	56.57 ± 0.34	10.97 ± 0.25	7.16 ± 0.21	
L-M50^-20	56.54 ± 0.36	10.95 ± 0.24	7.31 ± 0.23	
L-M65Bat	56.86 ± 0.35	6.96 ± 0.20	9.59 ± 0.26	

Table 3
Dissolution efficiency (%) of lignin samples in different solvents. Values are means ± standard deviations from duplicate measurements.

Samples labeling	Hexane	Ethanol	1,4-Dioxane	Acetone	Acetic acid
L-M35-3	4.0 ± 0.3	59.0 ± 1.8	71.0 ± 2.0	56.0 ± 1.6	73.0 ± 2.0
L-M35-18	4.0 ± 0.2	73.0 ± 2.0	82.0 ± 2.4	69.0 ± 1.9	96.0 ± 2.5
L-M50-3	7.0 ± 0.4	59.0 ± 1.7	82.0 ± 2.2	79.0 ± 2.0	83.0 ± 2.1
L-M50-18	4.0 ± 0.3	40.0 ± 1.5	75.0 ± 2.0	50.0 ± 1.7	30.0 ± 1.4
L-M65Bat	7.0 ± 0.5	86.0 ± 2.2	85.0 ± 2.1	90.0 ± 2.4	96.0 ± 2.0

the absence of hydrophobic moieties, consistent with MAHL containing more phenolic, carboxyl, and carbonyl, and other oxygenated functionalities. The HSQC spectra (Fig. 3) further support this interpretation. Intensified correlation peaks in the oxygenated aliphatic region (C—O, δC ≈ 60–90 ppm; δH ≈ 3.0–5.6 ppm) confirm the formation of new phenolic, carboxyl, and carbonyl groups during MAHF. Although these specific correlations are not included in Table 4, the observed decreases in β–*O*–4 linkages support ether cleavage, consistent with the increased abundance of oxygenated functionalities that enhance MAHL solubility in hydrogen-bonding, polar solvents.

L-M65Bat exhibited the highest solubility among all samples (86–96% in the four polar solvents), together with the lowest β–*O*–4 content (56.5%, Table 4) and the lowest Mw (Table 5), indicating extensive depolymerization and oxidation under the most severe MAHF conditions. These characteristics are consistent with its darkest coloration and the lowest L* value, reflecting the formation of highly conjugated chromophores and increased molecular polarity. In contrast, L-M50-18 exhibited reduced solubility despite prolonged reaction time, consistent with its higher molecular weight and clear evidence of condensation. Collectively, these results demonstrate that lignin solubility is governed by both molecular weight and functional group composition: depolymerized lignin enriched in –OH, –COOH, and –C=O groups exhibit higher solubility in polar media, whereas condensation and crosslinking diminish solubility. Therefore, carefully balancing depolymerization and condensation is critical for tuning lignin solubility and functional group composition for downstream applications.

3.4. Molecular weight of MAHL

Gel permeation chromatography (GPC) was used to characterize the molecular weight distribution of MAHL samples obtained under different conditions. The results reveal a strong correlation between MAHF severity, defined by reaction time and acid concentration, and the resulting lignin molecular weight profiles. The GPC chromatograms show a major peak accompanied by a shoulder at shorter elution times (Fig. S2A). This shoulder is barely visible for sample L-M35-3, which was collected under the mildest flow-through MAHF condition (M35T110) for 3 min. Increasing flow-through time increased lignin depolymerization, dissolution, and therefore yield, at the meantime, also induced lignin repolymerization/condensation. As a result, the shoulder became progressively more pronounced due to the formation of higher-molecular-weight components. In the sample collected from washing the final fractionated solids (L-M35Wa), the shoulder developed into a distinct second peak, clear evidence of lignin repolymerization. Additionally, the main peak gradually shifts to larger molecular weights (shorter elution times) with increasing flow-through time, further confirming the growing contribution of repolymerized lignin structures.

Increasing MA concentration enhanced the severity of MAHF and consequently increased lignin depolymerization and dissolution (Table S1), presumably due to more extensive ether bond cleavage. Comparison of GPC chromatograms for paired lignin samples collected at identical flow-through times indicates that a higher MA concentration promoted lignin repolymerization, as reflected by the more prominent shoulder in the GPC chromatograms (Fig. S2B). Under M50T110, this shoulder became a distinct second peak for lignin collected at a 9-min flow-through time. Increasing the flow-through time further shifted this second peak toward shorter elution times (higher molecular weights), suggesting progressively intensified lignin repolymerization.

At shorter flow-through times, such as 3 min, the main peak of the lignin obtained with 50 wt% MA (L-M50t-3) shifted slightly toward lower molecular weight when compared with its counterpart from the 35 wt% MA (L-M35-3). This indicates that higher acid concentration accelerated ether bond cleavage, resulting in more extensive initial depolymerization and thus lower-molecular-weight lignin fragments. Repolymerization during these very short reaction periods was minimal, especially at 35 wt% MA, as evidenced by the very weak shoulder (Fig. S2B).

The number-averaged (Mn) and weight-averaged (Mw) molecular weights, as well as the polydisperse index (PDI = Mn/Mw), were determined for all collected lignin samples (Table 5). The results clearly show increasing molecular weight and PDI with longer flow-through collection times, consistent with repolymerization-induced formation of a secondary peak discussed above.

3.5. Chemical structural of MAHL by 2D ^{1}H—^{13}C HSQC NMR

Two-dimensional (2D) ^{1}H—^{13}C HSQC NMR method provided information about the lignin chemical structural transformation during MAHF. The structural features, including aromatic unit composition (S- and G-units), S/G ratio, and major aliphatic interunit linkages (β–*O*–4, β–5, and β–β) were semi-quantitatively determined as summarized in Table 4, while representative spectra are shown in Fig. 3.

Birch TMP and MAHF water insoluble solids (WIS) samples, WIS-BM35f and WIS-BM50f, derived from birch wood chips, were compared with birch chips to evaluate the extent of structural modification. All samples displayed similar NMR data with high syringyl (S) content (80.6–81.6%) and low guaiacyl (G) content (18.4–19.4%), yielding elevated S/G ratios (4.16–4.43), consistent with hardwood lignin. WIS-BM35f and WIS-BM50f showed slightly higher S/G ratios compared to the birch chips (4.11%), suggesting slightly more removal of G-type lignin domains during MAHF. The β–*O*–4 contents of WIS-BM35f (91.6%) and BM50f (89.9%) were similar to that of birch chips (90.7%), indicating that MAHF under these conditions did not significantly cleave ether linkages in the WIS.

To investigate lignin solubility-related structural variations, WIS-BM35f and its corresponding soluble lignin (L-M35-3, L-M35-9, and L-M35-18) from MAHF were compared. The soluble lignin had significantly lower S-unit content (60.9–64.7%) and higher G-unit than the corresponding values of their WIS-BM35f, leading to lower S/G ratios (1.56–1.83). This trend suggests that G-rich fragments were more readily solubilized under MAHF, while S-rich domains were retained in the WIS fraction. The β–*O*–4 content decreased from 91.6% in WIS-BM35f to ~80% in the soluble lignin, confirming cleavage of ether linkages as a key solubilization mechanism. A similar pattern was observed between soluble lignin (L-M50-3, L-M50-9, and L-M50-18) obtained from MAHF with MA concentration 50 wt% and their WIS-BM50f. Soluble lignin had lower S/G ratios (1.78–2.11) and decreased β–*O*–4 contents (80.6–83.3%) than the corresponding value of WIS-BM50f (4.43 and 89.9%, respectively).

Comparisons between the soluble lignin from MAHF run BM35f with the corresponding lignin from BM50f at identical flow through time, e.g., L-M35-9 vs. L-M50-9, further revealed that higher acid concentration resulted in higher S/G ratios and slightly greater extent of lignin depolymerization and condensation as corroborated by molecular weight distribution measurements (Fig. S2B). This indicates enhanced dissolution of S-units accompanied by increasing cleavage and condensation

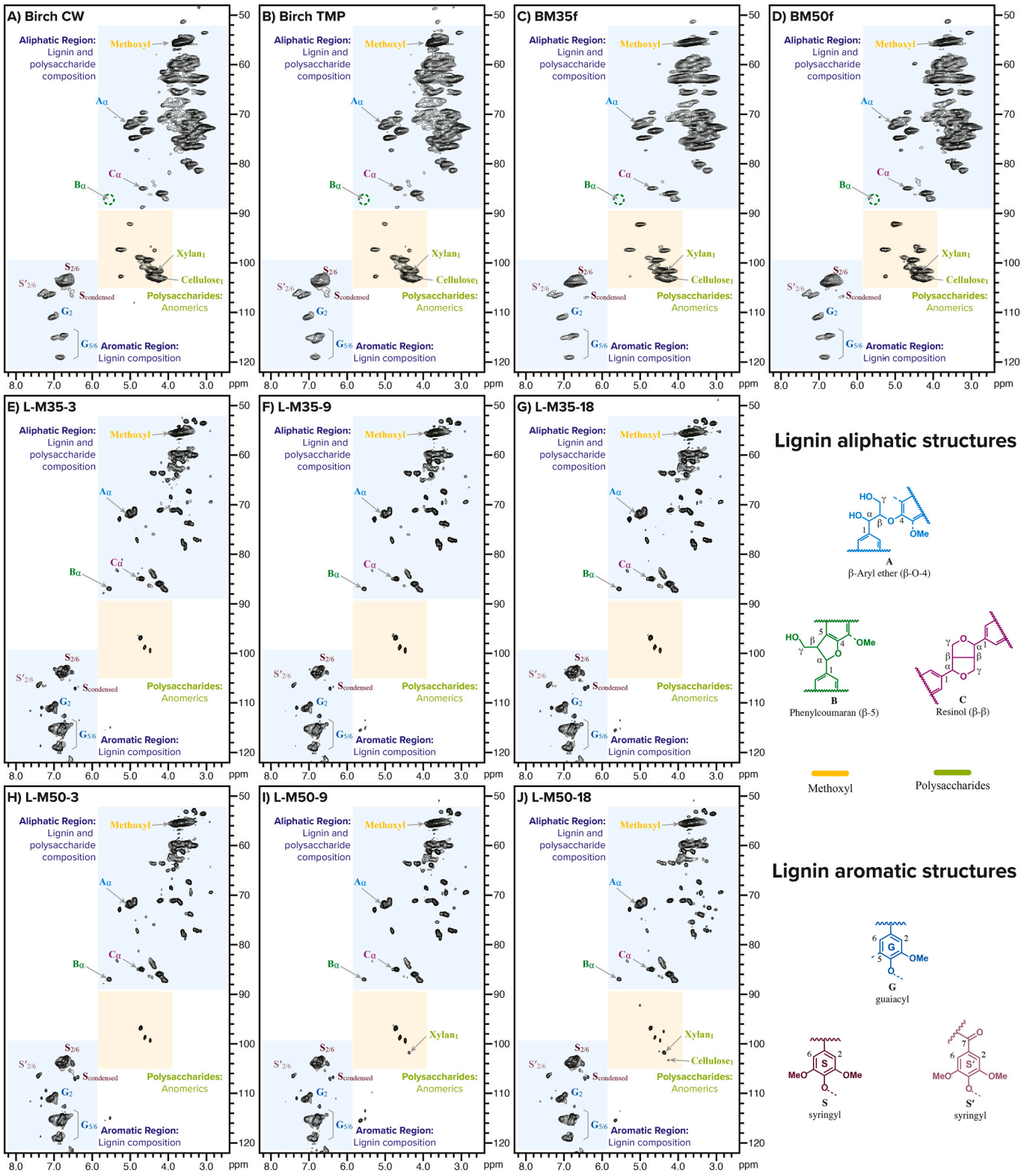

Fig. 3. 2D $^{1}H—^{13}C$ HSQC NMR spectra of selected lignin and WIS samples from different MAHF conditions in comparison with the spectra of birch wood and birch TMP. A: Birch wood chip; B: Birch TMP; C: WIS BM35f; D: WIS BM50f; E: L-M35-3; F: L-M35-9; G: L-M35-18; H: L-M50-3; I: L-M50-9; J: L-M50-18.

with elevated MA concentration. This trend was also observed when comparing lignin samples from the different collection times at the same MA concentrations, i.e., L-M35-3, L-M35-9, and L-M35-18, corroborated by molecular weight distribution (Fig. S2A).

The most severe batch fractionation using aspen wood at 65 wt% MA concentration, resulted in significant lignin (L-M65-bat) depolymerization and condensation with a drastically decreased β–*O*–4 content of 56.5%. This sample also exhibited elevated *S*-unit and carbon-carbon linkages (β–5 and β–β). In addition to the changes in inter-unit linkages, the 2D HSQC data revealed Hibbert's ketone structures, which arise from acid-catalyzed β–*O*–4 cleavage.

Table 4
Semi-quantitative analysis (interunit linkages, aromatic units, and S/G ratio) of WIS samples and MAHF dissolved lignin from integrating $^{1}H—^{13}C$ correlation peaks in the 2D HSQC spectra. Values are reported as percentages, except for the S/G ratio.

Samples	Aromatic units					Interunit linkages			
	S	$S_{Condensed}$	S_{Total}	G	S/G	β–*O*–4	β–5	β–β	HK*
Birch wood	75.86	4.58	80.44	19.56	4.11	90.71	2.05	7.24	–
Birch TMP	75.57	5.05	80.62	19.38	4.16	89.96	2.11	7.93	–
WIS-BM35f	76.35	4.92	81.27	18.73	4.34	91.59	1.11	7.30	–
WIS-BM50f	76.68	4.89	81.57	18.43	4.43	89.93	2.11	7.95	–
L-M35-3	59.20	1.70	60.91	39.09	1.56	80.33	9.21	10.46	–
L-M35-9	59.46	2.04	61.50	38.50	1.60	80.27	9.22	10.51	–
L-M35-18	62.18	2.53	64.71	35.29	1.83	82.55	7.53	9.92	–
L-M50-3	59.58	4.41	63.99	36.01	1.78	80.57	9.05	10.38	–
L-M50-9	62.27	2.88	65.15	34.85	1.87	82.24	7.59	10.17	–
L-M50-18	64.86	3.02	67.88	32.12	2.11	83.34	6.47	10.20	–
Aspen	68.03	0.29	68.33	31.63	2.16	88.75	3.00	8.25	–
WIS-AM65b	42.37	53.72	96.09	3.91	24.57	64.37	0.00	35.63	–
L-M65Bat	28.10	65.89	93.99	6.01	15.64	56.53	15.07	28.40	62.52

* HK: Hibbert's ketone. The data is presented on an β–O–4 + β–5 + β–β = 100% basis.

Table 5
Number (Mn) and weight-average (Mw) molecular weights and polydispersity index dispersity index PDI of lignin obtained from different F of birchwood TMP.

Samples	Mn (g/mol)	Mw (g/mol)	PDI
L-M35-3	1176	1312	1.74
L-M35-6	1181	1336	1.78
L-M35-9	1175	1314	1.75
L-M35-12	1192	1381	1.84
L-M35-15	1196	1383	1.82
L-M35-18	1178	1354	1.87
L-M35Wa	1323	1828	2.04
L-M50-3	1167	2206	1.89
L-M50-6	1175	2201	1.87
L-M50-9	1198	2428	2.03
L-M50-12	1314	3106	2.36
L-M50-15	1298	3169	2.44
L-M50-18	1342	3198	2.38
L-M65Bat	1111	1634	1.47
L-M50^-5	1157	2086	1.80
L-M50^-10	1180	2327	1.97
L-M50^-15	1252	2994	2.39
L-M50^-20	1352	3401	2.52

3.6. Application MAHL in sunscreen to improve UV-shielding

Selected light colored MAHL samples (Fig. S1) listed in Table 2 were supplemented into a commercial SPF 15 sunscreen at 5 wt% loading to demonstrate their potential for applications in skin care products. The colors and visual appearance of the lignin-containing sunscreens are shown in Fig. 4A in comparison with the control – the as purchased commercial SPF 15 sunscreen (without lignin). Except for the formulation using L-M65Bat, the sunscreens retained a light color. Even with the supplementation of only 5 wt% MAHL, the UV-shielding performances of the MAHL-containing sunscreens were greatly improved in general as shown in Fig. 4B, depending on lignin structure and molecular characteristics of MAHL added. The control commercial SPF 15 sunscreen exhibited UV transmittance of approximately 5% or more across both the UVB (290–320 nm) and UVA (320–400 nm) regions, indicating limited UV absorption capacity. Sunscreen formulations supplemented with MAHL exhibited lower UV transmittance except for the formulations with L-M35-3 in the wavelength range between 370 and 390 nm and L-M35-18 between 380 and 400 nm. It is worth to notice that the decrease in UV transmittance is very substantial for all the MAHL-supplemented formulations in the UVB range 290–320 nm in which photoprotection is critical for preventing sunburn or skin cancer due to the short wavelengths. It is also interesting to notice that the L-M50-3 blocked more than 99.5% the UV transmittance between 290 and 312 nm, exhibited the best performance among the five lignin-containing sunscreens evaluated.

In general, the lignin aromatic structure, phenolic hydroxyl groups, and conjugated double bonds act as natural chromophores to absorb light to provide UV blocking properties, particularly in the UVC and UVB ranges. Our earlier study indicated that MAHL of wheat straw and switchgrass from a more severe MAHF condition, with a greater extent of lignin carboxylation and condensation and more chromophoric groups, had a better UV absorption performance [37]. This corroborates existing studies on lignin chromophoric groups and condensation on UV shielding efficiency [10,11]. This also explains the poor performance of the sunscreen formulation using L-M35-3 from the run with low fractionation severity with low extent of condensation (reploymerization) and carboxylation. Studies also indicate that lignin miscibility with sunscreen and other factors such as lignin morphology can affect lignin-containing sunscreen UV protection performance [10,50]. As shown in Fig. 4A, the formulation with L-M50-3 and L-M35-18 have the best miscibility without visible large lignin particles, while the formulation

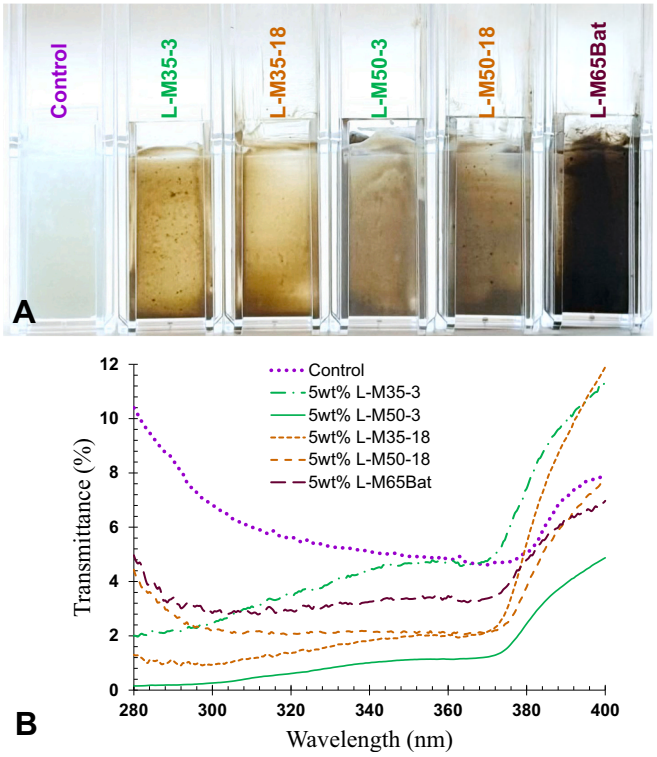

Fig. 4. A: Photos of MAHL supplemented sunscreens in comparison with the control (without lignin); B: comparisons of UV transmittance spectra across the UVB (290–320 nm) and UVA (320–400 nm) regions among a commercial SPF 15 sunscreen (control) and its MAHL-supplemented (at 5 wt%) sunscreen formulations using different lignin samples produced in the present study.

with L-M35-3 and L-M50-18 exhibited many lignin particles. SPF values (Table 6) calculated from the measured UV transmittance data further confirmed the enhancement of UV protection performance by lignin. Specifically, SPF increased to approximately 205 and 96 by supplementing 5 wt% of L-M50-3 and L-M35-18, respectively, far exceeding the values for both the control commercial sunscreen and other lignin-containing formulations. Very high SPF values of lignin containing sunscreens were also reported, for example, a SPF of 244 [51] using a chemically modified lignin and 130 using a pink colored lignin [52].

Light microscopic (LM) imaging provides more details about the morphology of the constituents of the lignin-containing sunscreens (Figs. 5, S3-S5) and substantiated the photographic imaging observations shown in Fig. 4A. Four types of LM images were taken, namely: (1) bright field (Fig. S3), (2) polarized light (Fig. S4), (3) epifluorescence with UV (361–389 nm) excitation and 435 nm long-pass fluorescence emission (Fig. 5), and (4) blue (465–495 nm) excitation and 525 nm long-pass emission (Fig. S5). Specifically, UV fluorescence with long pass emission LM shows the control commercial sunscreen (Fig. 5A) contains small particles with weak UV fluorescence. The sunscreens supplemented with L-M35-3 and L-M35-18 at 5 wt% contain lignocellulosic (fiber) fragments with relatively strong fluorescence as evidenced by the bright and large aspect-ratio patterns in Fig. 5B and C, also observed from the bright field LM (Fig. S3B and S3C) and polarized LM (Fig. S4B and C), and blue excitation fluorescence imaging (Fig. S5B and S5C), suggesting incomplete removal of carbohydrates by MAHF using a low MA concentration of 35 wt%. This is consistent with 2D-NMR analysis that showed carbohydrate peaks (Fig. 3E and G) in these two lignin samples (Fig. 3E and G). This was due to the less complete hydrolysis of hemicelluloses at the lower fractionation severities which resulted in dissolved lignin samples with higher carbohydrate contents. Furthermore, the sunscreen supplemented with L-M35-3 from the lowest severity contained more fiber fragments than the sunscreen L-M35-18 did, as evidenced by the birefringence patterns in the polarized LM (comparing Fig. S4B with S4C). The sunscreens supplemented with L-M50-18 and L-M65Bat contained large agglomerations presumably from lignin particles (Figs. S3E-F and S5E-F), suggesting lignin aggregation as seen from Fig. 4A. These large lignin aggregates were not birefringent (Fig. S4E-F) because lignin is amorphous. The sunscreen supplemented with L-M35-3 and L-M35-18 also contained many larger particular aggregates (~50–75 μm, Fig. S5B and C) than those seen in the control (Fig. S5A) and L-M50-3 (Fig. S5D). Consistent with that observed in Fig. S4A, the sunscreen with L-M50-3 and L-M35-18 exhibited the best dispersion within the commercial sunscreen (Fig. 5C and D), except for some lignocellulosic fiber fragments in the sunscreen supplemented with L-M35-18. In summary, the poor dispersion, the low lignin purity with high lignocellulosic fragments which decrease lignin content and cause poor dispersion, and the low UV shield capability of L-M35-3, and the large lignin particular aggregates of L-M50-18 and L-M65Bat resulted in low SPF values of the sunscreens supplemented with these three lignin samples. L-M50-3 with good dispersion and free of cellulosic fragments is best for sunscreen application and achieved the highest SPF of 205 (Table 6) at 5 wt% loading.

The results presented above suggest that supplement MAHL into sunscreen achieved outstanding UV-shieding performance without apparent limitations in terms of anti-UV capability. However, care needs to be taken in lignin dispersion to prevent lignin aggregation as aggregation and poor dispersion not only negatively affect UV protection performance but also appealing to consumers. Lignin toxicity studies and regulatory approval are of course needed before commercial adoption for skin care products.

3.7. Application of MAHL in wood adhesives

Four types of lignin wood adhesives were prepared in the present study as detailed in the experimental section: Lignin with water, lignin with formaldehyde (LF), lignin with phenol formaldehyde (LPF), and lignin formaldehyde with phenol formaldehyde (LFPF). For the formulation using lignin with water, two MAHLs L-M35 and L-M50 obtained at MA loadings 35% and 50%, respectively, were used in combination with double distilled water (ddH_2O) at MAHL: ddH_2O = 3:1 (w/w) to make the two pure lignin wood adhesives. The average dry strength (shortened as "bonding strength" in the following discussion) of the pure lignin adhesive using L-M50 obtained from pressing at 200 °C for 120 s was 2.51 MPa from triplicate experiments as shown in Fig. 6A and the wet strength was negligible. When pressing time was extended to 240 s, the average dry strength increased to 2.86 MPa, again with negligible wet strength. Decreasing pressing temperature below 200 °C resulted in negligible bonding strength.

The bonding strength of the pure lignin adhesives using L-M35 was improved even when pressing at temperatures below 200 °C. As shown in Fig. 6B, a bond strength of 3.01 MPa was obtained at pressing temperature of 180 °C for 120 s. Decreasing pressing time and temperature only slightly decreased bonding strength, i.e. to 2.58 MPa and 2.70 MPa under pressing at 180 °C for 60s and at 150 °C for 120 s, respectively. This is likely due to the fact that the L-M35 was more reactive as a result of low extent of lignin condensation under a mild MAHF condition. 2D-NMR analysis indicated that L-M35 contained less condensed S-unit compared with L-M50 (Table 4). When pressing at 150 °C for 60 s, however, dry bonding strength decreased to less than 1 MPa and wet strength was negligible. The low dry bonding strengths and negligible

Table 6
Sun protection factor (SPF) values of a commercial SPF 15 sunscreen (control) and formulations supplemented with different lignin at 5 wt% loading. Values are means ± standard deviations of 5 measurements of non-overlapping spots.

	Control	L-M35-3	L-M35-18	L-M50-3	L-M50-18	L-M65Bat
SPF	14 ± 1	40 ± 3	96 ± 6	205 ± 45	42 ± 3	33 ± 2

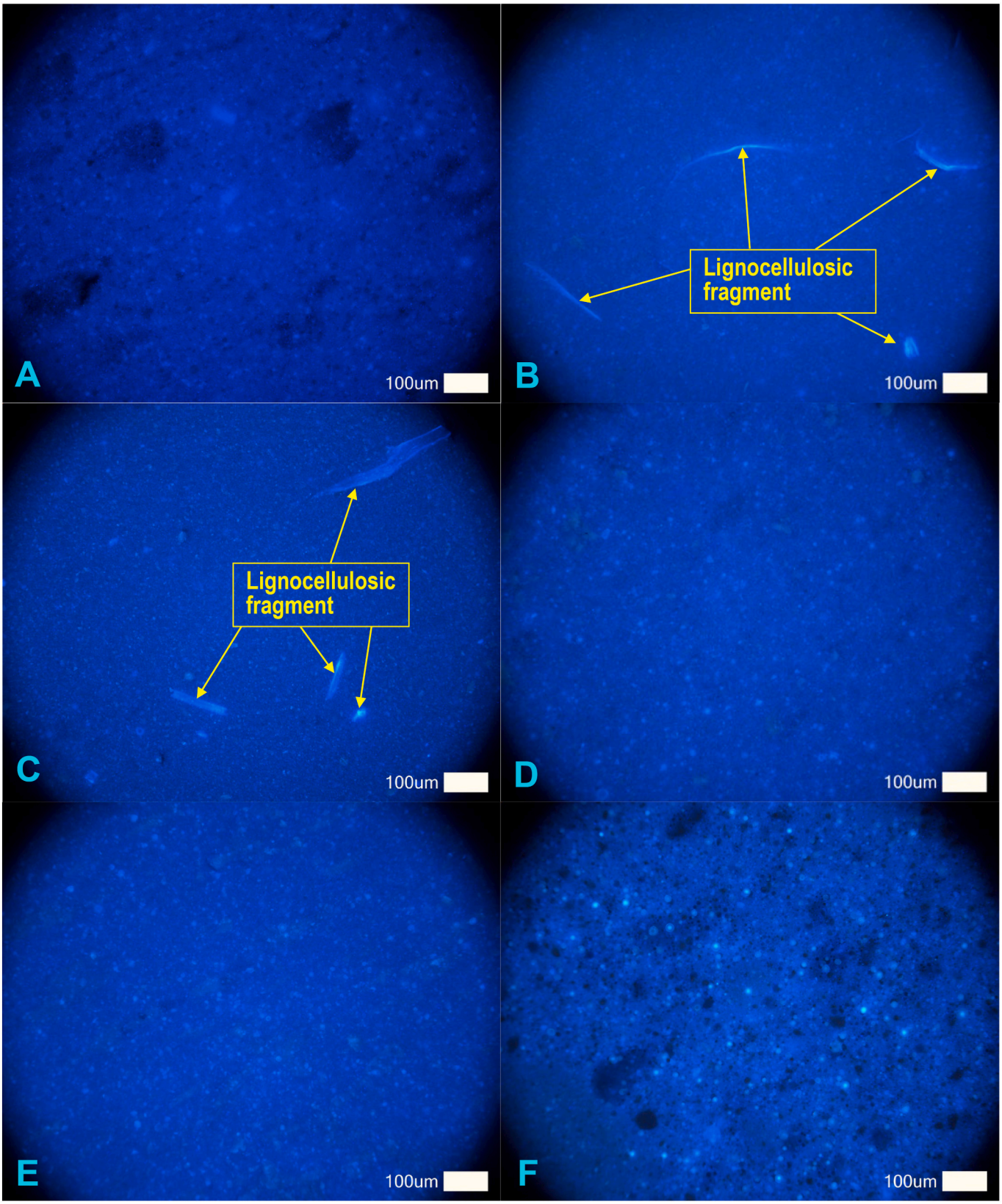

Fig. 5. UV (361–389 nm) excitation and 435 nm long pass fluorescence microscopy of the lignin-containing sunscreens in comparison with a commercial sunscreen (Control, no lignin) showing strong blue fluorescence from lignocellulosic fragments. A: Control; B: L-M35-3; C: L-M35-18; D: L-M50-3; E: L-M50-18; F: L-M65Bat. Exposure was optimized to give maximum intensity just below 255 nm. Sunscreens (A) and (D) received about 2 times longer exposure compared to (B) through (E). Large lignocellulosic particles (arrows) can be seen in (B) and (C).

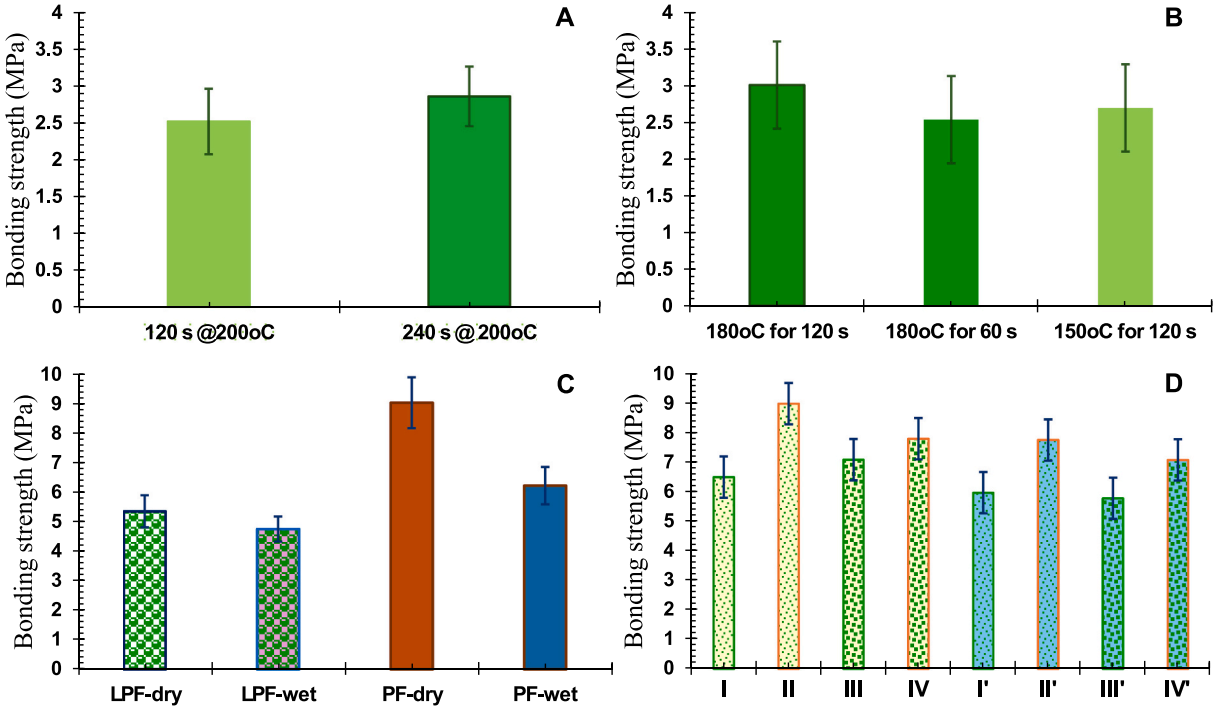

Fig. 6. Bonding strength (lap shear bond strength) of different MAHL wood adhesive formulations under various pressing conditions, based on at least triplicate measurements. A-B: Pure lignin adhesives made of MAHL L-M50 (A) and L-M35 (B) with ddH2O. C: Lignin phenol formaldehyde (LPF) adhesive vs phenol formaldehyde (PF) made of MAHL L-M50 pressing at 150 °C for 120 s. D: Lignin formaldehyde phenol formaldehyde (LFPF) adhesive made of MAHL L-M50 LF. I–IV are all dry samples: (I): 10% LF with 90% PF, pressing at 150 °C and for 120 s; (II) same as I but pressing at 180 °C; (III) pressing same as I but 20% LF with 80% PF; (IV) same as III but pressing at 180 °C. I′–IV' are wet samples corresponding to I–IV, respectively.

wet strengths of pure lignin adhesives are well known [9].

Lignin samples L-MA35 and L-MA50 were each reacted with formaldehyde to produce stronger lignin adhesives, LF. Both the dry and wet bonding strength of the resultant LF were tested using four wood samples. The average dry strength was 3.83 MPa and the wet strength was 3.05 MPa when pressing at 180 °C for 120 s. The reaction of lignin with formaldehyde improved the lignin reactivity so that the adhesive can polymerize during bond formation and therefore bond the wood [53–55]. Although syringyl (*S*)-type units dominate the lignin structure (~80%), guaiacyl (G) units (~20%) play a critical role in reactivity, as they participate in condensation reactions and react with formaldehyde through the C5 position. Syringyl units, despite having an additional methoxy group, can also undergo condensation at the C2 and C6 positions under these reaction conditions. Therefore, both S and G units contribute to crosslinking and network formation in the adhesive system, supporting the observed bonding performance [15].

The LPFs tested here were made of lignin/PF ratios of 10:90 wt% and 20:80 wt%. The amounts of 10 wt% and 20 wt% of lignin added to PF were chosen because these low amounts of substitution would be easier to implement in commercial adhesives. Four wet and four dry samples were tested. In comparison with the bonding strengths of PF adhesive, the dry and wet strengths of the LPF with 10% L-MA50 were 5.31 MPa and 4.15 MPa, respectively, when pressing at 150 °C for 120 s as shown in Fig. 6C. This wet strength of over 3 MPa obtained using ASTM D7998 indicates good potential to pass the North American standards for interior plywood [56].

Previous research has shown the benefits of reacting lignin with formaldehyde [54,57], so it made sense to combine LF with PF to form LFPF. Both a 10% and a 20% substitution of PF by LF (using L-MA50) were tested (Table 1). Both LFPFs with the 10% and the 20% substitutions were pressed at 180 °C and 150 °C for 120 s in wet and dry tests (Fig. 6D). The average dry strength for the 10% LF substitution LFPF adhesive was 6.50 MPa when pressing at 150 °C based on triplicate testing. The dry strength increased to 9.0 MPa when pressing at 180 °C. This significant increase in adhesive bonding strength is probably due to a more complete cure at the higher temperature, as this PF formulation, unlike commercial formulas, does not have any catalysts to accelerate or lower the temperature of cure. Even with 20% LF substitution (L-MA50), dry bonding strength remained very high at 7.86 and 7.09 MPa when pressing at 180 °C and 150 °C respectively (Fig. 6D). The test results also show that the LFPF adhesives have great wet strength of near 6.0 MPa or greater. These wet strengths are far above the minimums typically needed for interior applications. Both the dry strength and wet strength of LFPF are similar to those of PF (comparing Fig. 6D with C). The great bonding strength of over 7 MPa at 20% substitution suggests 30 to 40% substitution may be applied in future testing.

The temperature of the cure exotherm and the Delta H of the PF and LPF adhesives were determined by DSC. The PF adhesive had an exothermic peak at 151.5 °C and a Delta H of 196 J/g. Adding lignin to the PF at 10% and analyzing by DSC resulted in an exothermic peak at 155 °C with a Delta H of 168 J/g. Adding lignin to the PF increased the cure temperature and decreased the Delta H, which explains the lower dry and wet strengths of the LPF adhesive than those of the PF.

In summary, the performance MAHL is satisfactory only under partial substitution of key ingredients of existing wood adhesives, but not complete substitution. Even using protection chemistry [5,12] to prevent lignin condensation with improved lignin reactivity [9], a higher pressing temperature is needed to achieve satisfactory results.

4. Conclusions

This study revealed the unique physical and chemical properties of maleic acid hydrotropic fractionation dissolved wood lignin (MAHL) in terms of color, dissolution efficiency in different organic solvents, molecular weight distribution, and chemical structures. Moderate fractionation produced MAHLs with light color, relatively low molecular

weight, low extent of repolymerization or condensation and therefore good reactivity, and good solubility in polar solvents. These unique physical and chemical properties are favorable for valorization through direct polymeric applications. Specifically, MAHLs with a relatively low amount of carbohydrates and low extent of lignin particle aggregation can be directly mixed with commercial sunscreens to substantially enhance UV shielding capability. Sun protection factor (SPF) values of MAHL-containing sunscreens increased from 14 (control without lignin) up to 205 with just 5 wt% lignin supplementation. Lignin purity (carbohydrate content), lignin aggregation and dispersion in sunscreen, and the UV blocking capability of the lignin itself all played important roles. MAHL from mild fraction with good reactivity are ideally suited to produce lignin-based wood adhesives. MAHL at 10% loading with phenol formaldehyde (LPF) resulted in an adhesive that could potentially pass the North American standards for interior plywood based on the ASTM D7998 test. Lignin formaldehyde (LF) with phenol formaldehyde (LFPF) at 20% LF substitution resulted in a wet bonding strength near 6 MPa pressing at 150 °C for 120 s, suitable for interior applications and suggesting greater LF substitution can be applied.

CRediT authorship contribution statement

Xiaoxue Zhang: Methodology, Investigation, Data curation, Writing – original draft. **Noah Altschuler:** Investigation, Data curation, Writing – original draft. **Linda F. Lorenz:** Supervision, Resources, Methodology, Investigation, Funding acquisition, Data curation, Writing – original draft. **Peter Kitin:** Visualization, Methodology, Investigation, Writing – original draft. **Christopher G. Hunt:** Supervision, Resources, Methodology, Formal analysis, Writing – original draft. **Hoon Kim:** Visualization, Methodology, Investigation, Formal analysis, Data curation, Writing – original draft. **Clayton Mickles:** Methodology, Investigation, Formal analysis, Data curation, Writing – original draft. **Jiansong Chen:** Methodology, Investigation, Formal analysis. **Xuejun Pan:** Validation, Supervision, Resources, Methodology, Writing – review & editing. **J.Y. Zhu:** Supervision, Resources, Project administration, Methodology, Funding acquisition, Formal analysis, Conceptualization, Writing – review & editing, Writing – original draft.

Declaration of competing interest

Author Zhu is a co-inventor of a US patent on maleic acid hydrotropic fractionation technology.

Acknowledgements

This work was supported by the U.S. Department of Agriculture (USDA), Forest Service which made Zhang's visiting appointment at the USDA Forest Products Laboratory (FPL) possible. The findings and conclusions in this publication are those of authors and should not be construed to represent any official USDA or U.S. Government determination or policy. We acknowledge Carlos Baez at the Analytical Chemistry and Microscopy Lab at FPL conducted chemical composition analysis.

Appendix A. Supplementary data

Supplementary data to this article can be found online at https://doi.org/10.1016/j.ijbiomac.2026.154518.

Data availability

Data will be made available on request.

References

[1] R. Rinaldi, R. Jastrzebski, M.T. Clough, J. Ralph, M. Kennema, P.C.A. Bruijnincx, B. M. Weckhuysen, Paving the way for lignin valorisation: recent advances in bioengineering, biorefining and catalysis, Angew. Chem. Int. Ed. 55 (29) (2016) 8164–8215, https://doi.org/10.1002/anie.201510351.
[2] G. Gellerstedt, E.L. Lindfors, Structural changes in lignin during kraft pulping, Holzforschung 38 (3) (1984) 151–158.
[3] K.P. Kringstad, R. Mörck, ^{13}CNMR spectra of kraft lignins, Holzforschung 37 (5) (1983) 237–244.
[4] S. Constant, H.L.J. Wienk, A.E. Frissen, P.d. Peinder, R. Boelens, D.S. van Es, R.J. H. Grisel, B.M. Weckhuysen, W.J.J. Huijgen, R.J.A. Gosselink, P.C.A. Bruijnincx, New insights into the structure and composition of technical lignins: a comparative characterisation study, Green Chem. 18 (9) (2016) 2651–2665, https://doi.org/10.1039/C5GC03043A.
[5] L. Shuai, M.T. Amiri, Y.M. Questell-Santiago, F. Héroguel, Y. Li, H. Kim, R. Meilan, C. Chapple, J. Ralph, J.S. Luterbacher, Formaldehyde stabilization facilitates lignin monomer production during biomass depolymerization, Science 354 (6310) (2016) 329–333, https://doi.org/10.1126/science.aaf7810.
[6] S. Van Den Bosch, W. Schutyser, R. Vanholme, T. Driessen, S.F. Koelewijn, T. Renders, B. De Meester, W.J.J. Huijgen, W. Dehaen, C.M. Courtin, B. Lagrain, W. Boerjan, B.F. Sels, Reductive lignocellulose fractionation into soluble lignin-derived phenolic monomers and dimers and processable carbohydrate pulps, Energy Environ. Sci. 8 (6) (2015) 1748–1763, https://doi.org/10.1039/C5EE00204D.
[7] I. Kumaniaev, E. Subbotina, J. Sävmarker, M. Larhed, M.V. Galkin, J.S.M. Samec, Lignin depolymerization to monophenolic compounds in a flow-through system, Green Chem. 19 (24) (2017) 5767–5771, https://doi.org/10.1039/c7gc02731a.
[8] Z. Wang, S. Qiu, K. Hirth, J. Cheng, J. Wen, N. Li, Y. Fang, X. Pan, J.Y. Zhu, Preserving both lignin and cellulose chemical structures: flow-through acid hydrotropic fractionation (AHF) at atmospheric pressure for complete wood valorization, ACS Sustain. Chem. Eng. 7 (2019) 10808–10820, https://doi.org/10.1021/acssuschemeng.9b01634.
[9] G. Yang, Z. Gong, X. Luo, L. Chen, L. Shuai, Bonding wood with uncondensed lignins as adhesives, Nature 621 (7979) (2023) 511–515, https://doi.org/10.1021/acsomega.4c00452.
[10] M.H. Tran, D.P. Phan, E.Y. Lee, Review on lignin modifications toward natural UV protection ingredient for lignin-based sunscreens, Green Chem. 23 (13) (2021) 4633–4646, https://doi.org/10.1039/d1gc01139a.
[11] Y. Qian, X. Qiu, S. Zhu, Lignin: a nature-inspired sun blocker for broad-spectrum sunscreens, Green Chem. 17 (1) (2015) 320–324, https://doi.org/10.1039/C4GC01333F.
[12] S. Bertella, M. Bernardes Figueirêdo, G. de Angelis, M. Mourez, C. Bourmaud, E. Amstad, J.S. Luterbacher, Extraction and surfactant properties of glyoxylic acid-functionalized lignin, ChemSusChem 15 (15) (2022) e202200270, https://doi.org/10.1002/cssc.202200270.
[13] S. Zheng, S. Sun, L.P. Manker, J.S. Luterbacher, Aldehyde-stabilization strategies for building biobased consumer products around intact lignocellulosic structures, Acc. Chem. Res. 58 (6) (2025) 877–892, https://doi.org/10.1021/acs.accounts.4c00819.
[14] M. Talebi Amiri, G.R. Dick, Y.M. Questell-Santiago, J.S. Luterbacher, Fractionation of lignocellulosic biomass to produce uncondensed aldehyde-stabilized lignin, Nat. Protoc. 14 (3) (2019) 921–954, https://doi.org/10.1038/s41596-018-0121-7.
[15] L. Shuai, Y.M. Questell-Santiago, J.S. Luterbacher, A mild biomass pretreatment using γ-valerolactone for concentrated sugar production, Green Chem. 18 (4) (2016) 937–943, https://doi.org/10.1039/C5GC02489G.
[16] Q. Song, F. Wang, J. Cai, Y. Wang, J. Zhang, W. Yu, J. Xu, Lignin depolymerization (LDP) in alcohol over nickel-based catalysts via a fragmentation-hydrogenolysis process, Energy Environ. Sci. 6 (3) (2013) 994–1007, https://doi.org/10.1039/C2EE23741E.
[17] M.Y. Balakshin, E.A. Capanema, I. Sulaeva, P. Schlee, Z. Huang, M. Feng, M. Borghei, O.J. Rojas, A. Potthast, T. Rosenau, New opportunities in the valorization of technical lignins, ChemSusChem 14 (4) (2021) 1016–1036, https://doi.org/10.1002/cssc.202002553.
[18] J. Wang, Y. Deng, Y. Qian, X. Qiu, Y. Ren, D. Yang, Reduction of lignin color via one-step UV irradiation, Green Chem. 18 (3) (2016) 695–699, https://doi.org/10.1039/C5GC02180D.
[19] J. Zhang, Z. Tian, X.X. Ji, F. Zhang, Light-colored lignin extraction by ultrafiltration membrane fractionation for lignin nanoparticles preparation as UV-blocking sunscreen, Int. J. Biol. Macromol. 231 (2023) 123244, https://doi.org/10.1016/j.ijbiomac.2023.123244.
[20] H. Zhang, F. Chen, X. Liu, S. Fu, Micromorphology influence on the color performance of lignin and its application in guiding the preparation of light-colored lignin sunscreen, ACS Sustain. Chem. Eng. 6 (9) (2018) 12532–12540, https://doi.org/10.1021/acssuschemeng.8b03464.
[21] H. Zhang, Y. Bai, B. Yu, X. Liu, F. Chen, A practicable process for lignin color reduction: fractionation of lignin using methanol/water as a solvent, Green Chem. 19 (21) (2017) 5152–5162, https://doi.org/10.1039/C7GC01974B.
[22] H. Zhang, X. Liu, S. Fu, Y. Chen, High-value utilization of kraft lignin: color reduction and evaluation as sunscreen ingredient, Int. J. Biol. Macromol. 133 (2019) 86–92, https://doi.org/10.1016/j.ijbiomac.2019.04.092.
[23] H. Wikberg, T. Ohra-Aho, J. Leppavuori, T. Liitia, H. Kanerva, Method for Producing Reacting Lignin, World Intellectual Property Organization, 2018. WO 2018/115592 A1.

[24] P. Widsten, T. Tamminen, T. Liitiä, Natural sunscreens based on nanoparticles of modified kraft lignin (CatLignin), ACS Omega 5 (22) (2020) 13438–13446, https://doi.org/10.1021/acsomega.0c01742.
[25] H. Zhang, Y. Bai, W. Zhou, F. Chen, Color reduction of sulfonated eucalyptus kraft lignin, Int. J. Biol. Macromol. 97 (2017) 201–208, https://doi.org/10.1016/j.ijbiomac.2017.01.031.
[26] A. Zhang, X. Wu, X. Ouyang, H. Lou, D. Yang, Y. Qian, X. Qiu, Preparation of light-colored lignosulfonate sunscreen microcapsules with strengthened UV-blocking and adhesion performance, ACS Sustain. Chem. Eng. 10 (29) (2022) 9381–9388, https://doi.org/10.1021/acssuschemeng.2c01487.
[27] F. Cheng, S. Liu, S.D. Karlen, H. Kim, F. Lu, J. Ralph, L.M. Vázquez Ramos, G. W. Huber, J.A. Dumesic, Poplar lignin structural changes during extraction in γ-valerolactone (GVL), Green Chem. 25 (1) (2023) 336–347, https://doi.org/10.1039/D2GC03446H.
[28] L. Chen, J. Dou, Q. Ma, N. Li, R. Wu, H. Bian, D.J. Yelle, T. Vuorinen, S. Fu, X. Pan, J.Y. Zhu, Rapid and near-complete dissolution of wood lignin at ≤80 °C by a recyclable acid hydrotrope, Sci. Adv. 3 (9) (2017) e1701735, https://doi.org/10.1126/sciadv.1701735.
[29] C. Cai, K. Hirth, R. Gleisner, H. Lou, X. Qiu, J.Y. Zhu, Maleic acid as a dicarboxylic acid hydrotrope for sustainable fractionation of wood at atmospheric pressure and ≤100 °C: mode and utility of lignin esterification, Green Chem. 22 (5) (2020) 1605–1617, https://doi.org/10.1039/C9GC04267A.
[30] S. Jeong, J. Ryu, Q. Yang, J.Y. Zhu, C.G. Yoo, Recent advances in hydrotropic solvent systems for lignocellulosic biomass utilization, Green Chem. 26 (4) (2024) 1806–1830, https://doi.org/10.1039/d3gc03309k.
[31] J.Y. Zhu, X. Pan, Efficient sugar production from plant biomass: current status, challenges, and future directions, Renew. Sust. Energ. Rev. 164 (2022) 112583, https://doi.org/10.1016/j.rser.2022.112583.
[32] K. Ganesan, J. Sternberg, S. Pilla, Green chemistry design of one-step extraction of multi-functionalized lignin-precursors directly from biomass, Green Chem. (2026), https://doi.org/10.1039/D5GC02571K.
[33] A.R. Procter, A review of hydrotropic pulping, Pulp Pap. Mag. Can. 72 (8) (1971) 67–74.
[34] H.Y. Mou, E. Heikkilä, P. Fardim, Topochemistry of alkaline, alkaline-peroxide and hydrotropic pretreatments of common reed to enhance enzymatic hydrolysis efficiency, Bioresour. Technol. 150 (2013) 36–41, https://doi.org/10.1016/j.biortech.2013.09.093.
[35] C. Cai, J. Li, K. Hirth, G.W. Huber, H. Lou, J.Y. Zhu, Comparison of two acid hydrotropes for sustainabl fractionation of birch wood, ChemSusChem 13 (2020) 4649–4659, https://doi.org/10.1002/cssc.202001120.
[36] X. Zhang, P. Kitin, J. Geng, H. Kim, R. Gleisner, D. Yelle, J.Y. Zhu, Carboxylated lignin-containing cellulose microfibrils produced from wood at high solids through maleic acid hydrotropic fractionation, ACS Sustain. Chem. Eng. 14 (17) (2026) 8421–8435, https://doi.org/10.1021/acssuschemeng.6c01405.
[37] C. Su, X. Wang, K. Hirth, M. Arvanitis, Y. Cao, G. Fang, J.Y. Zhu, Bioactive lignin from maleic acid hydrotropic fractionation: revealing the structural–bioactivity relationship, Int. J. Biol. Macromol. 302 (2025) 140519, https://doi.org/10.1016/j.ijbiomac.2025.140519.
[38] W.G. Glasser, About making lignin great again—some lessons from the past, Front. Chem. 7 (2019), https://doi.org/10.3389/fchem.2019.00565.
[39] A.J. Ragauskas, G.T. Beckham, M.J. Biddy, R. Chandra, F. Chen, M.F. Davis, B. H. Davison, R.A. Dixon, P. Gilna, M. Keller, P. Langan, A.K. Naskar, J.N. Saddler, T. J. Tschaplinski, G.A. Tuskan, C.E. Wyman, Lignin valorization: improving lignin processing in the biorefinery, Science 344 (6185) (2014), https://doi.org/10.1126/science.1246843.
[40] Q. Ma, K. Hirth, H. Zhai, J.Y. Zhu, Highly bleachable wood fibers containing less condensed lignin from acid hydrotropic fractionation (AHF), ACS Sustain. Chem. Eng. 8 (2020) 9046–9057, https://doi.org/10.1021/acssuschemeng.0c02129.
[41] A. Sluiter, B. Hames, R. Ruiz, C. Scarlata, J. Sluiter, D. Templeton, D. Crocker, Determination of Structural Carbohydrates and Lignin in Biomass Laboratory Analytical Procedure (LAP), NREL Technical Report NREL/TP-510-42618 (Version 07-08-2011), 2011.
[42] H. Kim, J. Ralph, T. Akiyama, Solution-state 2D NMR of ball-milled plant cell wall gels in DMSO-d_6, Bioenergy Res. 1 (2008) 55–62.
[43] H. Kim, J. Ralph, Solution-state 2D NMR of ball-milled plant cell wall gels in DMSO-d_6/pyridine-d_5, Org. Biomol. Chem. 8 (3) (2010) 576–591, https://doi.org/10.1039/B916070A.
[44] H. Kim, J. Ralph, A gel-state 2D-NMR method for plant cell wall profiling and analysis: a model study with the amorphous cellulose and xylan from ball-milled cotton linters, RSC Adv. 4 (15) (2014) 7549–7560, https://doi.org/10.1039/C3RA46338A.
[45] ASTM, Standard Test Method for Measuring the Effect of Temperature on the Cohesive Strength Development of Adhesives using Lap Shear Bonds under Tensile Loading, ASTM Standard Test Method D7998-19, 2019, https://doi.org/10.1520/D7998-19.
[46] W. Schutyser, T. Renders, S. Van den Bosch, S.F. Koelewijn, G.T. Beckham, B. F. Sels, Chemicals from lignin: an interplay of lignocellulose fractionation, depolymerisation, and upgrading, Chem. Soc. Rev. 47 (3) (2018) 852–908, https://doi.org/10.1039/C7CS00566K.
[47] N. Li, Y. Li, C.G. Yoo, X. Yang, X. Lin, J. Ralph, X. Pan, An uncondensed lignin depolymerized in the solid state and isolated from lignocellulosic biomass: a mechanistic study, Green Chem. 20 (18) (2018) 4224–4235, https://doi.org/10.1039/C8GC00953H.
[48] Z. Gong, L. Shuai, Lignin condensation, an unsolved mystery, Trends Chem. 5 (3) (2023) 163–166, https://doi.org/10.1016/j.trechm.2022.12.005.
[49] E. Melro, L. Alves, F.E. Antunes, B. Medronho, A brief overview on lignin dissolution, J. Mol. Liq. 265 (2018) 578–584, https://doi.org/10.1016/j.molliq.2018.06.021.
[50] Y. Zhang, M. Naebe, Lignin: a review on structure, properties, and applications as a light-colored UV absorber, ACS Sustain. Chem. Eng. 9 (4) (2021) 1427–1442, https://doi.org/10.1021/acssuschemeng.0c06998.
[51] Y. Wu, Y. Qian, A. Zhang, H. Lou, D. Yang, X. Qiu, Light color dihydroxybenzophenone grafted lignin with High UVA/UVB absorbance ratio for efficient and safe natural sunscreen, Ind. Eng. Chem. Res. 59 (39) (2020) 17057–17068, https://doi.org/10.1021/acs.iecr.9b06970.
[52] X. Chen, X. Li, Y. Xiao, L. Ding, L. Liu, R. Qu, Y. Han, Y. Qian, Preparation of light-colored botanical sunscreen from pink birch lignin, ChemSusChem 18 (13) (2025) e2202500454, https://doi.org/10.1002/cssc.202500454.
[53] A. Ait Benhamou, L. Abid, I. Calvez, A. Cloutier, M. Nejad, T. Stevanovic, V. Landry, Advances in lignin chemistry, bonding performance, and formaldehyde emission reduction in lignin-based urea-formaldehyde adhesives: a review, ChemSusChem 18 (16) (2025) e202500491, https://doi.org/10.1002/cssc.202500491.
[54] P. Nafisah, E. Wibowo, M. Mubarok, W. Darmawan, M. Lubis, A. Santoso, S. Kusumah, S. Afif, B.-D. Park, The role of lignin in enhancing adhesion performance and reducing formaldehyde emissions of phenol resorcinol–formaldehyde resin adhesives, Int. J. Biol. Macromol. 323 (2025) 147251, https://doi.org/10.1016/j.ijbiomac.2025.147251.
[55] D. Zhao, Z. Li, Y. Zhang, P. Fu, The role of lignin in adhesives for lignin-based formaldehyde-based resins: a review, Biomass Convers. Biorefinery 15 (11) (2025) 16307–16341, https://doi.org/10.1007/s13399-024-06397-1.
[56] C.R. Frihart, C.G. Hunt, Protein structure and wood adhesives, Ind. Crop. Prod. 229 (2025) 121008, https://doi.org/10.1016/j.indcrop.2025.121008.
[57] M. Siahkamari, D. Debnath, T. Wang, M. Nejad, A fundamental study of lignin reactions with formaldehyde and glyoxal, Green Chem. 27 (2025) 2342–2358, https://doi.org/10.1039/D4GC05695G.